Unravelling mechanism for detecting chromium on functionalized gold nanoparticles *via* a smartphone and spectrophotometric-based systems supported by CIEL*a*b* colour space and molecular dynamics

Sindisiwe F. Muthwa [a], Nontuthuko S. Zulu [a], Marcel Kistan [a], Stanley C Onwubu [a], Ndivhuwo P. Shumbula [b], Nosipho Moloto [b], Siyasanga Mpelane [c], Thulani Hlatshwayo [d], Mbuso Mlambo [d e], Phumlani S. Mdluli [a,e,*]

[a]Department of Chemistry, Durban University of Technology, P O Box 1334, Durban 4000, South Africa
[b]Molecular Sciences Institute, School of Chemistry, University of the Witwatersrand, Private Bag 3, Wits, 2050, South Africa
[c]Analytical Facility, University of Johannesburg, P.O. Box: 524, Auckland Park 2006, South Africa
[d]Department of Physics, University of Pretoria, Pretoria 0002, South Africa
[e]Nanotechnology Innovation Centre, Health Platform, Advanced Materials Division, Mintek, Randburg, South Africa

*Corresponding author. Email: phumlanem@mintek.co.za

Highlights

- Synthesis of citrate stabilized gold nanoparticles and the displacement of citrate ions by DPC on the surface of gold nanoparticles to form DPC-AuNPs.
- The use of RGB colour coordinates and CIELa*b* colour system to analyse colour changes upon the addition of Cr (VI) standards in the concentration range of 0.5–50.0 µM.
- Molecular dynamics simulation of DPC-AuNPs interaction with Cr (VI), resulting to DPC-Cr (VI) confirming the aggregation of AuNPs.

Abstract

This paper demonstrates the application of smartphones as well as spectrophotometers as tools to demystify the mechanism leading to colour variation of 1,5-diphenylcarbazide functionalized gold nanoparticles (DPC-AuNPs) due to chromium addition. Colour Grab 3.6.1 app was used to capture and decode colours from samples containing DPC-AuNPs with different concentrations of hexavalent Chromium [Cr(VI)] standards. The presence of Cr(VI) aggregated DPC-AuNPs resulted in a colour change from pink to blue and a decrease in the peak intensity as accompanied by a red shift of the SPR peak to 670 nm.

The R colour coordinates decreased as Cr(VI) concentration was increased to 16 µM then a rapid decrease was noted between 18–25 µM and G and B colour coordinates followed the same trend. Colour difference (ΔE) increased significantly as the Cr(VI) concentration increased. A rapid decrease was noticed in the hue angle between 16–25 µM while chroma decreased significantly as the Cr(VI) concentration increased. Molecular dynamics calculation of a gold cluster was used to simulate the aggregation process. The calculated radial distribution [g(r)] from cluster models of the Cr-DPC complex was two-fold more than Cr-AuNPs. This was associated with the aggregation of gold nanoparticles leading to the appearance of the blue colour of AuNPs solution which was also supported by the intensity obtained from colour Grab. This study will potentially be applied in the future for the fabrication of a Lovibond photometer for the detection of metal ions in environmental samples.

Graphical abstract

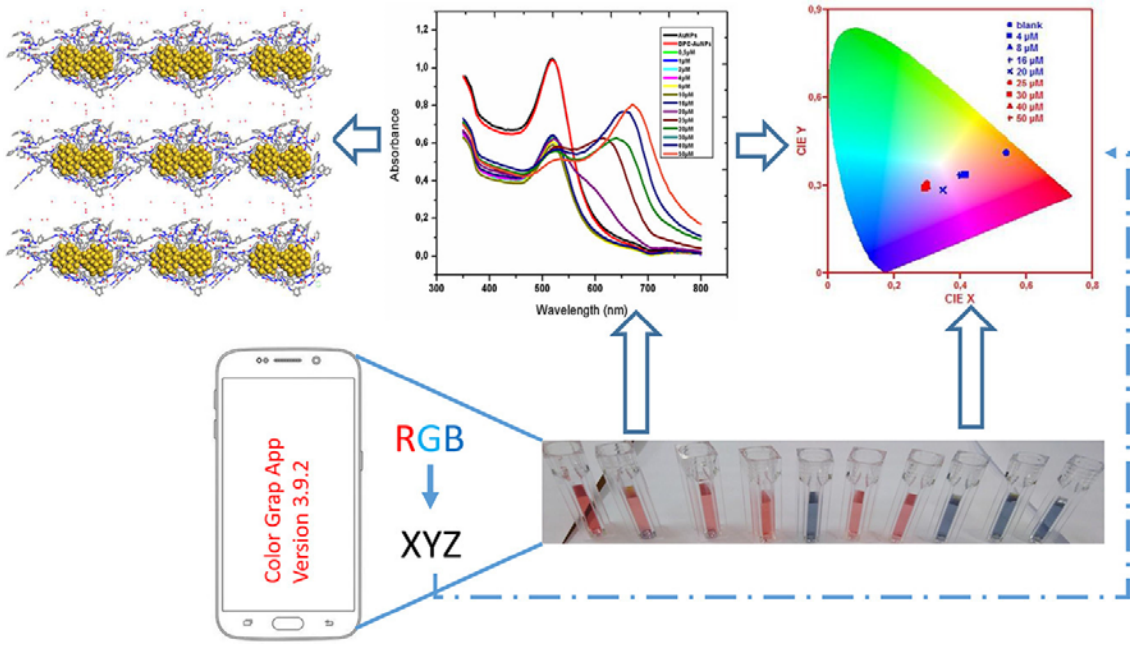

Keywords: Chromaticity diagram; Gold nanoparticles; Hexavalent chromium; 5-Diphenylcarbazide; Colorimetry

1. Introduction

The detection of hexavalent chromium from wastewater and other environmental samples using the UV–Visible spectrometric technique is an established method [1,2]. However, with the advancement of nanotechnology and nanoscience, there has been a growing trend of using gold nanoparticles (AuNPs) for the detection of metal ions. The application of AuNPs is mainly contributed by their characteristic surface Plasmon resonance (SPR) properties that are highly dependent on the particle's size, shape and inter-particle distance [3], [4], [5], [6]. The AuNP-based colorimetric sensors are of particular interest because they are exploited on the colour change that arises from the inter-particle Plasmon coupling upon the aggregation of AuNPs (changing colour from red to blue or purple) [7], [8], [9], [10], [11], [12]. Over the past decade, the controlled assembly and disassembly of AuNPs have been a subject of great interest due to the prospective applications, such as the one reported by Shaikh et al. on the application of citrate-capped AuNPs functionalized with ortho-dicarboxylate substituted pyridine (2,3-PDCA) to probe the stability of AuNPs and response for Cr(III) [13]. Further studies by Lai and Tseng resulted in a simple and rapid method for sensing Cr(VI) using 5-thio-(2-nitrobenzoic acid) modified AuNPs (TNBA-AuNPs) as well as a remedial removal of Cr(III), and as a sensor for Cr(VI) [14]. Shahrivari et al. reported the interaction of 4-amino-5-methyl-4H-1,2,4-triazole-3-thiol functionalized AuNPs (AMTT-Au NPs) with some metal cations [15]. These examples demonstrated how functionalized AuNPs can be used to detect different substances with good selectivity and sensitivity [16].

Molecular dynamics (MD) simulation has proved to be the most convenient tool to complement experimental results. MD simulations are suitable for studying gold nanocluster systems to expose nano-structure features with or without assuming any prior specific gold nanocluster

models [17], [18], [19], [20]. Our previous study demonstrated the impact of interatomic distance to understand the adsorption of polymers on gold nanoclusters [17]. In a separate study, we demonstrated that theoretical simulations could provide good evidence for the interaction of silver and gold with pyrrolidone, which was also supported by experimental data [21]. The simulated gold nanoclusters provided good evidence to understand the mechanism between silver clusters and polyvinyl pyrrolidone (PVP). The study also demonstrated the regioselective adsorption of the selected functional group of PVP onto the surface of gold nanoclusters.

Another smartphone-based colorimetric system has been reported for the detection of different analytes using metal nanoparticles [22], [23], [24], [25]. In the current study, we particularly explore the effects of chromium ions on inducing aggregation of gold nanoclusters models through classical MD simulations and chromaticity diagrams. Special focus attention was on the radial distribution factor of chromium interaction with DPC, hence a series of MD simulations were carried out for gold nanocluster capped with 1.5-diphenylcarbazide (DPC) with the addition of chromium ions. We also report the image analysis using CIEL*a*b* and Red Green Blue (RGB) coordinates for the colorimetric detection of Cr(VI) using AuNPs functionalized with DPC. A Smartphone was used as well to analyse the intensity of colours to support the spectrophotometric technique.

2. Materials and methods

2.1. Chemicals and materials

Gold chloride trihydrate (>99.9%) was purchased from Leap Chem (Hangzhou, China) through DLD Scientific (Durban, South Africa). Other chemicals used were tri-sodium citrate dehydrate (>99%) from Merck (Pty) Ltd (Durban, South Africa) and Potassium dichromate from Associated Chemical Enterprises (Johannesburg, South Africa). Other reagents were of analytical grade and used without further purification. All solutions were prepared with deionized water (18.2 MΩcm specific resistance). All chemicals that were used for synthesis were purchased from Sigma-Aldrich and Merck (St. Louis, Missouri United States) and used without further purification. The solvents used were of synthesis grade.

2.2. Instrumentation

UV–Vis extinction spectra were measured on a Cary UV 50 from Varian (Cape Town, South Africa) spectrophotometer at room temperature. All Localised Surface Plasmon Resonance (LSPR) spectra were recorded from 350 to 800 nm and experimental absorbence was measured at 520 and 650 nm. Transmission Electron Microscopy (TEM) observations were carried out with a TEM CM 120 model from Philips (Johannesburg, South Africa). The TEM was operated, and images were processed at 120 kV. The melting point was determined by Stuart SMP 10 (Palo Alto, California) and was uncorrected.

2.3. Analysis of the intensity of colours using a smartphone

A Mobicel R6 smartphone was used to capture the intensity of each gold standard. The colour Grab app version 3.8.1 developed by Loomatix Ltd was installed and used to analyse the intensity of gold nanoparticles. The RBG values that were obtained from the colour Grab app were converted to the XYZ chromaticity diagram.

2.4. Computational simulations

The relative surface-to-molecule orientation on gold nanoclusters was modelled following our published work with minor alterations [20]. In this case, AuNPs with diameters of 0.5 nm (cluster sizes Au43) were constructed (Fig. 4) and surfactant adsorption was simulated using the Metropolis Monte Carlo method and surfactants were allowed to be adsorbed onto the AuNP surfaces [26]. Since a trade-off exists between simulation accuracy and computational time, it becomes increasingly more difficult to accurately execute molecular mechanics and dynamics calculations on large gold clusters. Therefore, the Au43 small nanocluster was selected and simulated to reduce simulating cost and time. It was found that for the largest nanocluster, the computational time (wall-clock time) became too large to continue. However, although these simulated nanocluster sizes were not the same size as those used in the experimental investigation because of the cost of calculation, the same trends can still be observed as discussed below. Molecular mechanics were used to determining the optimum geometries for each of the resulting DPC, DPC–AuNP systems, and MD simulations were performed on each of the systems to arrive at the energy-optimized configurations. The Condensed-phase Optimized Molecular Potentials for Atomistic Simulation Studies (COMPASS) force field was used to calculate the intermolecular potential energy of DPC-AuNP complexes. The models indicating the absorption of DPC were generated using the amorphous cell construction of Material Studio as well as the COMPASS force field. The lattice parameters' cell dimensions were set at $a = b = c = 36.40$ Å. The COMPASS force field is the first *ab initio* forcefield that enables accurate and simultaneous prediction of gas-phase properties (structural, conformational, vibrational, and so on) and condensed-phase properties (equation of state, cohesive energies, and so on) for inorganic materials. All systems were subjected to energy minimization using the Forcite module in Biovia Material Studio 2020 before MD simulations were conducted. The following convergence criteria were set to fine as follows, energy = 1×10^{-4} kcal/mol, Max. force = 0.005 kcal/mol/Å and Maximum displacement = 0.001 Å.The MD simulation using Forcite Dynamics calculation at constant temperature and constant volume (NVT) thermodynamic ensembles which lasted for 50 picoseconds with a time step of 1 femtosecond and all atomic density profiles were collected in the last 50 picoseconds simulated MD results for each model. All MD simulations were performed in triplicates, snapshots of the simulated data are shown in Supplementary Table S1.

3. Results and discussion

3.1. Sensitivity of the response of DPC-AuNPs to Cr(VI)

The digital image from colour Grab App and the change in the colours of the DPC-AuNPs upon the addition of Cr (VI) standards solutions in the concentration range of 0.5–50.0 μM are presented in Fig. 1 and Supplementary Fig. S1.

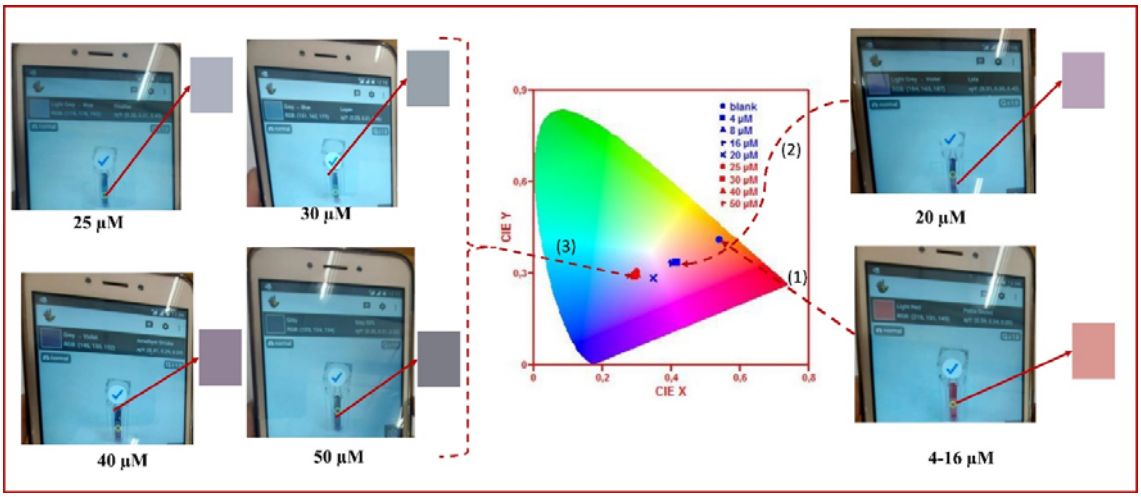

Fig. 1. Photograph images of the DPC-AuNPs blank and different concentrations of Cr(VI) in the range of 0.5–50.0 µM, captured by smartphone using colour Grab as well as the corresponding Chromaticity diagram associated with each generated coluor.

The colour change of the DPC-AuNPs induced by Cr(VI) was monitored using the smartphone colour Crab App and UV–Vis spectrophotometry. The colour grab App generated different colours upon the addition of different concentrations of Cr(VI) onto DPC-AuNPs. The change in colour from red to blueish was associated with the formation of anisotropic nanoparticles, and the alteration of the dielectric environment of the surface of AuNPs as shown in Supplementary Fig. S1 (a). These observations were confirmed with a UV–Vis spectrophotometer which showed two well-separated peaks at 520 and 670 nm as shown in Supplementary Fig. S1 (b). Further observation of the colour change upon increasing the concentration of Cr was observed from the UV–Vis spectra which showed that the addition of 20 µM Cr(VI) led to a slight red shift to 670 nm wavelength. The result of the colour Grab for 20 µM Cr(VI) was converted into an observable colour using the RGB values, this generated a clear violet colour which confirmed that an increase in the Cr(VI) concentration over 20 µM contributed to a second peak at 670 nm wavelength and a parallel decrease in the intensity of the SPR peak at 520 nm was observed as shown in Supplementary Fig. S1 (b). Thus, the colour of the DPC-AuNPs changed from Ruby-red to blue as the Cr(VI) concentration was increased [Supplementary Fig. S1 (a)]. The created colour pattern for the Cr(VI) standards matched the colours of the solutions. The TEM image in Supplementary Fig. S1(c) showed that the synthesised gold nanoparticles were monodispersed with an average diameter of 14 nm. The DPC-AuNPs have been utilized as a sensor for the detection of Cr(VI) as shown in Table 1. It was found that the detection limit in environmental samples was 0.3 µM [27]. In Table 1, other methods are shown where a comparison of the AuNPs' sizes, and gold conjugates gave a variable limit of detections (LOD). In the current study, further employment of the chromaticity diagram was explored to probe colour development due to aggregation as a result of the complexation of Cr(VI) by DPC-AuNPs.

Table 1. Data on the analytical methods of the reported gold nanoparticles-based methods for the determination of chromium.

Gold nanoparticles size (nm)	Capping Agent	Methods	LOD	Ref
13	1,5-diphenylcarbazide	Photometric	0.3 µM	[27]
20	Monoclonal antibodies against isothiocyanobenzyl-EDTA (iEDTA)-chelated Cr^{3+}	immunochromatographic assay	50 ng/mL	[28]
19.5	sodium hyaluronate	Colorimetric	2.90 nM	[29]
14	3-(p-tolyl)-2,3-dihydropyrazolo[3,4-b]indole-1(4H)-carbothioamide	Colorimetric	0.14 µM	[6]
13	Tween 20	Colorimetric	0.009 µM	[7]
10	Dithiocarbamate-modified N-benzyl-4-(pyridine-4-ylmethyl)aniline ligand	Colorimetric	31 ppb	[30]
13	5-thio-(2-nitrobenzoic acid)	Colorimetric	1 µM	[14]

3.2. Image analysis using RGB colour coordinates and CIELa*b* colour system

The RBG values were obtained from colour Grab analysis, these were generated from the colours of AuNP's response to the concentration of Cr(VI) as shown in Fig. 2 and Supplementary Fig. S2, respectively. A significant decrease for the red colour component was observed in both curves, however, this was slightly prominent in the UV–Vis spectrum as shown in Supplementary Fig. S1(b). The significant decrease in red colour was associated with the increased Cr(VI) concentration which led to more aggregation, thus, indicating the colour change of AuNPs from red to blue. Meanwhile, the green and blue curves were gradually increased as the concentration of Cr(VI) was increased from 0 to16 µM. However, there was a significant decrease from 18–50 µM to lower values of green and blue, respectively as shown in Fig. 2 and Supplementary Fig. S2(a). The RGB colour coordinates were used to generate the CIE L*a*b* colour system coordinates which were further used to create the chromaticity diagram. Supplementary Fig. S2 (b) represents the hue angle and chroma of the data that was obtained from the CIE L*a*b* colour system. It was noted that there was a decrease in the hue angle as observed from the Cr(VI) concentration of 0–20 µM. The decrease in the L values suggested that there was a change from lightness (red) to darkness (blue) which was associated with the aggregation of AuNPs as shown in Fig. 2(b). A notable a* curve significantly decreased; this trend was again associated with the change from the red region (+a) to a green region (–a). The observation obtained from the b* curve showed that for the Cr(VI) concentration from 0–16 µM, the b* curve was almost constant, then an observable decrease was noted for Cr(VI) concentration ranging from 18 to 20 µM. This was associated with the colour change of AuNPs from red to blue. These results agreed with the data obtained from the spectrophotometer which are presented in Supplementary Fig. S1(b)

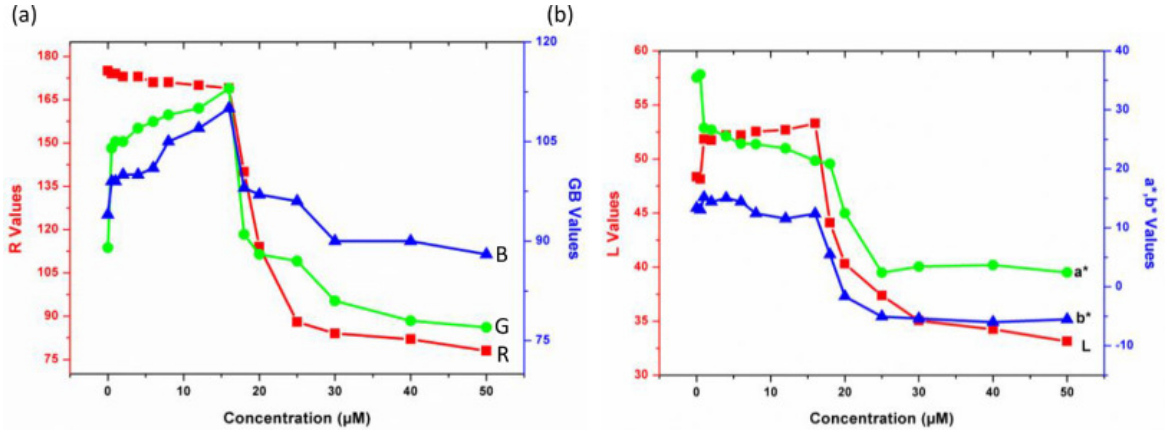

Fig. 2. (a) RBG colour plot against the corresponding Cr(VI) concentration and (b) plots of L*a*b* against Cr(VI) concentration.

3.3. Qualitative and quantitative analysis of the response of DPC-AuNPs to Cr(VI)

The colour difference (ΔE) was calculated using equation 1 (supp. Information) with the values of ΔL, Δa* and Δb* obtained from the colour produced on the calibration standards shown in Supplementary Fig. S1 (a). Fig. 3(a) and Supplementary Fig. S2(a) show that the ΔE value increased significantly with increasing Cr(VI) concentration which confirmed high assay reproducibility due to the aggregation of AuNPs. The colour change associated with ΔE value is very instrumental in understanding the design of the Lovibond colour filters for detecting chromium in water. These colour changes which were measured were associated with the modulus of the distance vector between the initial colour values and the actual colour coordinates. The Hue angle (h*) was considered the qualitative attribute of colour. The Hue angle was used to define the difference between a certain colour concerning a grey colour with the same lightness. Hue was calculated using equation 2 (supp. Information) and the obtained values are plotted against the concentration of Cr(VI) in Fig. 2(b). A significant decrease of the Hue angle was observed in the concentration of chromium ranging from 18–25 μM. Chroma (C*) was also used as the quantitative attribute of the change in colour due to the aggregation of AuNPs. The higher C* values were associated with the high colour intensity of samples perceived by human eyes.The C* was calculated using equation 3 (Supp Information). The C* decreased significantly with the increase in Cr(VI) concentration up to 25 μM with dullness of 4.260 and vividness of 35.908 as shown in Supplementary Fig. S2(b). Total colour difference and C* were considered the most sensitive parameters for the measurement of colour. The final horseshoe chromaticity diagram is shown in Fig. 3(a) for data obtained from the smartphone as well as in Supplementary Fig. S2(c) for spectrophotometric data. It was visible from the plotted RBG point in the chromaticity diagram that the increased concentration of chromium contributed to the colour change from red to blue, which is due to the aggregation of AuNPs as shown in pathways 1 and 2 of Fig. 3. Further evidence of the aggregation is shown in the plotted chromaticity diagram that shows the shifting toward the blue region [Fig. 3(a)]. The mechanism of aggregation is due to the formation of the Cr(VI) DPC complex thus leaving unprotected AuNPs inducing aggregation due to the sintering. In Fig. 3, it was noted that as the concentration of chromium ions was increased, the XY coordinates obtained from RBG coordinates occupied the blue region of the chromaticity diagram model, further evidence of this trend was also observed in Supplementary Fig. S2(c) from spectrophotometric data.

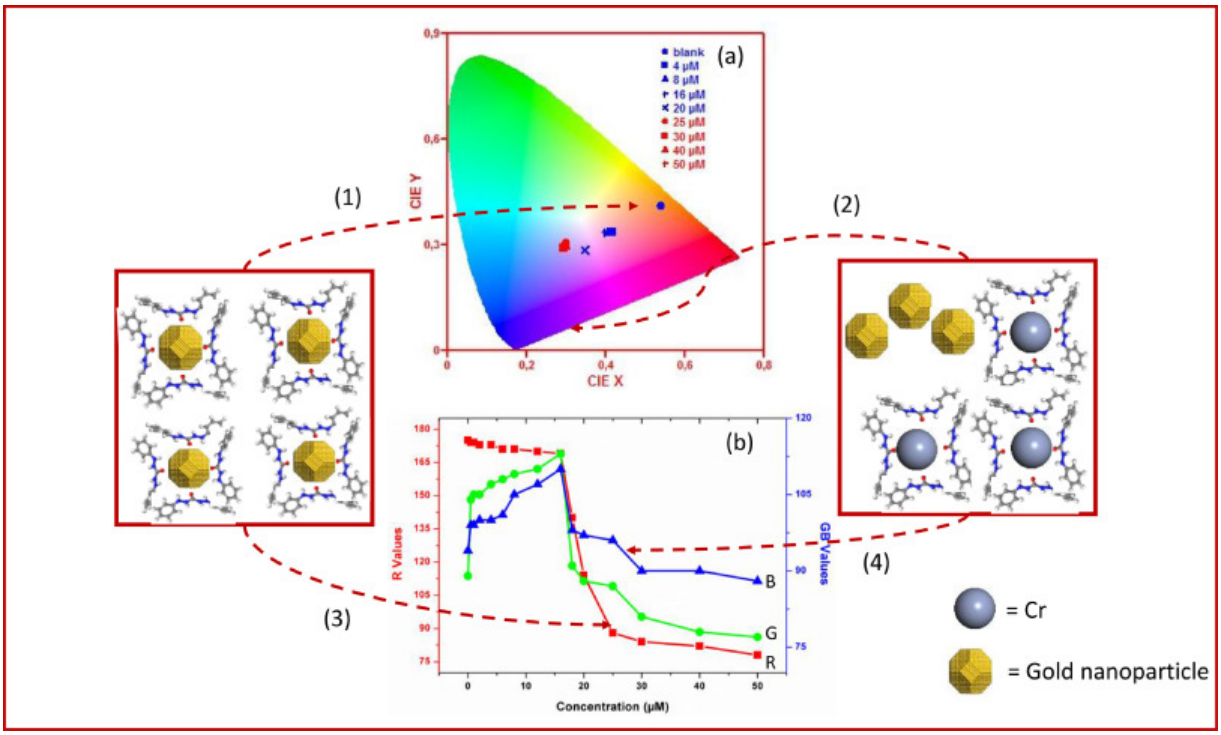

Fig. 3. Three pathways leading to aggregation of gold nanoparticles (1) position of aggregated gold nanoparticles in the Chromaticity and (2) enhanced blue values as a result of aggregation, and (3) position in chromaticity image of dispersed gold nanoparticles.

3.4. Molecular simulation of DPC-AuNPs to Cr(VI)

The model depicting the aggregation of DPC-AuNPs upon the addition of Cr(VI) is shown in Fig. 4. The charges of Cr(VI) were balanced with oxygen as shown with the red dots in Fig. 4(b). Fig. 4 demonstrates that upon the addition of Cr(VI), aggregation was induced which could be seen in Fig. 4(b) as compared to Fig. 4(a) where gold clusters are separated. The mechanism of aggregation was discussed in our previously published work [6,31].The mechanism is due to the interaction of Cr(VI) with the capping DPC which is introduced by replacing the citrate used during the synthesis of AuNPs. This results in the formation of the Cr-DPC complex, thus leaving AuNPs uncapped as a result, aggregation is induced as shown in Fig. 4(b).

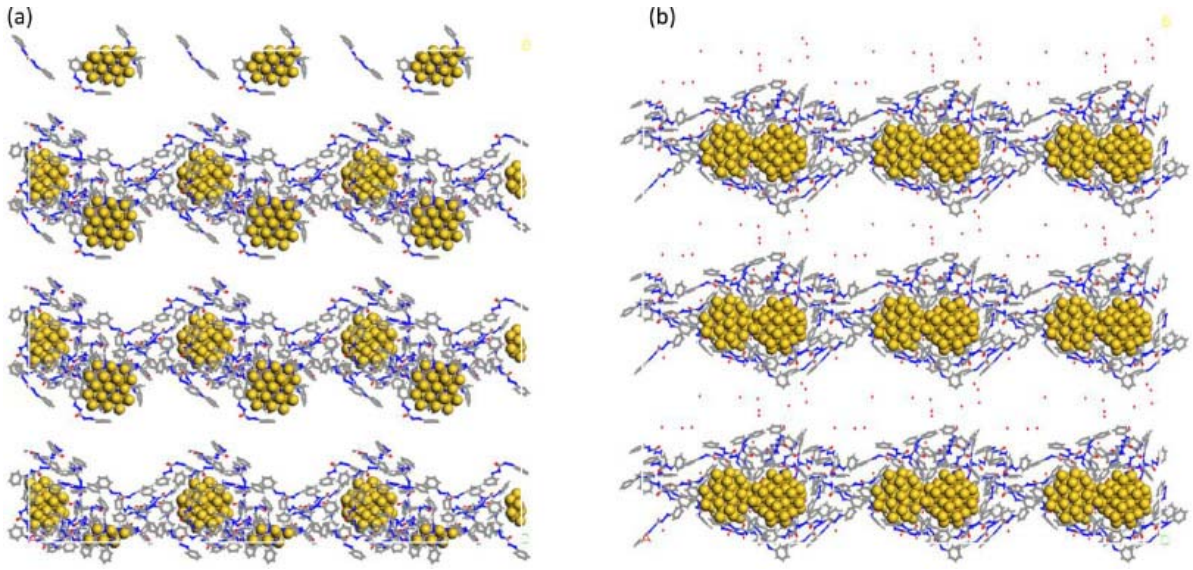

Fig. 4. Model for simulation DPC-AuNPs and Cr(IV) (a) DPC-AuNPs and (b) Cr-DPC-AuNPs.

The MD simulation was performed in triplicate, it is evident from the calculated radius of gyration that there is a slightly different in the final calculated data, however, it was noted that they all fall between 3.5 to 4.5 Å (Supplementary Fig. S3 and Supplementary Table S1). The simulated radial distribution functions (RDF) for different selected atoms of DPC-AuNPs and Cr(IV) were calculated to quantify interactions amongst the DPC groups, AuNPs, and Cr ions. The RDF provided information regarding the intermolecular interaction amongst the three components (AuNPs, Cr and DPC). The peak height and position were used for the structural analysis of these interactions. The RDF of DPC-AuNPs is shown in Fig. 5(a), in this case, the simulation was done by interacting AuNPs with the carbonyl end of the DPC. In Fig. 5(a), it can be noted that the r(Å) at 3 Å is associated with RDF [g(r)] of 3.4 r, this is an indication of strong interaction with the surface of gold nanoparticles, where most of the DPC molecules are within 3 Å from the surface of gold nanoparticles. A further molecular simulation was done to depict the formation of a new Cr-DPC complex. The formation Cr-DPC complex was simulated by looking at the bonds between Cr-N and Cr-AuNP bond formation using the radial distribution as shown in Fig.s 5(a) and (b). Clear evidence of the formation of a strong Cr-N bond, leading to the formation of the Cr-DPC complex is evident from the radial distance of 3 Å. The height of the g(r) for Cr-AuNPs is 3.4 r at the radial distribution of 3 Å. Notable so, the radial distance at 3 Å for the Cr-DPC bond is 8.4 r. It is obvious from Fig. 5(c) that the radial distribution for Cr-DPC was increased by more than two folds when it is compared with the radial distribution of Cr-AuNPs. This demonstrated clear evidence of the formation Cr-DPC complex. The formation of this complex was very crucial in understating the aggregation process of AuNPs. The mechanism of this process can be explained by the process that is similar to the molecule exchange process wherein AuNPs are stabilized by DPC which covers the surface, thus preventing aggregation. However, upon the addition of Cr(VI) ions into the system, they interact with DPC, leaving uncapped AuNPs which are likely to aggregate as attested with the simulated radial distribution functions in Fig. 5.

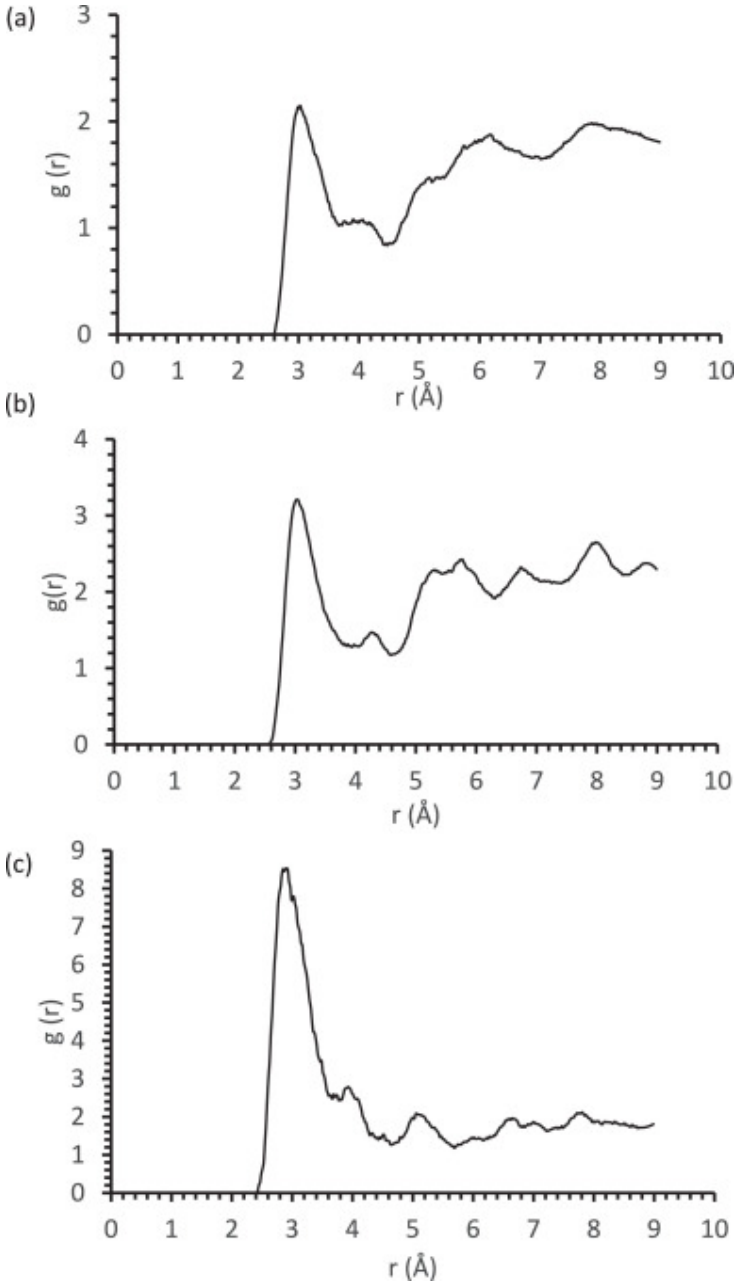

Fig. 5. Radial distribution function for DPC-AuNPs and Cr(IV) (a) DPC-AuNPs, (b) Cr-AuNPs and (c) Cr-DPC.

4. Conclusions

This study demonstrated the elucidation and full explanation of the mechanism for aggregation of DPC-AuNPs supported by chromaticity diagram as well molecular modelling. The result of this study showed that the colour change leading to the formation of a blue complex is due to the aggregation of AuNPs as a result of the formation of a complex between DPC and Cr (VI). The application of the CIEL*a*b* colour system and RGB colour coordinates may assist in understanding the colorimetric method used for the detection of Cr(VI) and other metal ions in water bodies. The use of colour difference (ΔE) was appropriate for a colorimetric

concentration measurement based on the colour change due to the DPC-AuNPs aggregation. The combination of the DPC-AuNPs and image analysis based on ΔE enabled quantitative analysis for multiple colour changes as expected. The present method will accelerate applications of colorimetric systems to point-of-care testing and in resource-limited settings. The aggregation of AuNPs was further proved by using MD simulation.

CRediT authorship contribution statement

Sindisiwe F. Muthwa: Conceptualization, Methodology. **Nontuthuko S. Zulu:** Writing – original draft. **Marcel Kistan:** Writing – original draft. **Stanley C Onwubu:** Writing – review & editing. **Ndivhuwo P. Shumbula:** Writing – review & editing. **Nosipho Moloto:** Writing – review & editing. **Siyasanga Mpelane:** Resources. **Thulani Hlatshwayo:** Writing – review & editing. **Mbuso Mlambo:** Writing – review & editing. **Phumlani S. Mdluli:** Writing – review & editing, Supervision, Funding acquisition.

Declaration of Competing Interest

The authors declare the following financial interests/personal relationships which may be considered as potential competing interests.

Acknowledgments

We would like to acknowledge Mintek, the National Research Foundation (South Africa), ESKOM Tertiary Education Support Programme (South Africa) and Moses Kotane Institute as well as the Centre for Higher Computer Performance in Cape Town for financial support and providing computational resources for this research.

Data availability

No data was used for the research described in the article.

References

1. A. Lace, D. Ryan, M. Bowkett, J. Cleary, Chromium monitoring in water by colorimetry using optimised 1,5-diphenylcarbazide method, Int. J. Environ. Res. Public Health 16 (10) (2019) 1803.
2. A. Sanchez-Hachair, A. Hofmann, Hexavalent chromium quantification in solution: comparing direct UV–visible spectrometry with 1,5-diphenylcarbazide colorimetry, C. R. Chim. 21 (9) (2018) 890–896.
3. J. Guo, D. Huo, M. Yang, C. Hou, J. Li, H. Fa, H. Luo, P. Yang, Colorimetric detection of Cr (VI) based on the leaching of gold nanoparticles using a paper-based sensor, Talanta 161 (2016) 819–825.
4. S.K. Tripathy, J.Y. Woo, C.-.S. Han, Colorimetric detection of Fe (III) ions using label-free gold nanoparticles and acidic thiourea mixture, Sensors Actuators B: Chem. 181 (2013) 114–118.
5. X. Wu, Y. Xu, Y. Dong, X. Jiang, N. Zhu, Colorimetric determination of hexavalent chromium with ascorbic acid capped silver nanoparticles, Anal. Methods 5 (2) (2013) 560–565.

6. S.F. Muthwa, T.R. Makhanya, M. Mlambo, N.P. Shumbula, P.M. Shumbula, S.C. Onwubu, N. Moloto, R.M. Gengan, P.S. Mdluli, Synthesis and characterization of 3-(p-tolyl)-2, 3-dihydropyrazolo [3, 4-b] indole-1 (4H)-carbothioamide functionalized gold nanoparticles for the CIEL∗ a∗ b∗ /Yxy colorimetric detection of Cr (VI), (2020) 127985.
7. X. Wang, Y. Wei, S. Wang, L. Chen, Red-to-blue colorimetric detection of chromium via Cr (III)-citrate chelating based on Tween 20-stabilized gold nanoparticles, Colloids Surfaces A: Physicochem. Eng. Aspects 472 (2015) 57–62.
8. B. Shilpa, Pyridoxal derivative functionalized gold nanoparticles for colorimetric determination of zinc(ii) and aluminum (iii), RSC Adv. 5 (118) (2015) 97690–97695.
9. S. Bothra, R. Kumar, S.K. Sahoo, Pyridoxal conjugated gold nanoparticles for distinct colorimetric detection of chromium(iii) and iodide ions in biological and environmental fluids, N. J. Chem. 41 (15) (2017) 7339–7346.
10. T. Lou, L. Chen, C. Zhang, Q. Kang, H. You, D. Shen, L. Chen, A simple and sensitive colorimetric method for detection of mercury ions based on anti-aggregation of gold nanoparticles, Anal. Methods 4 (2) (2012) 488–491.
11. A. Safavi, R. Ahmadi, Z. Mohammadpour, Colorimetric sensing of a silver ion based on an anti aggregation of gold nanoparticles, Sensors Actuators B: Chem. 242 (2017) 609–615.
12. Y.-.M. Sung, S.P. Wu, Highly selective and sensitive colorimetric detection of Ag (I) using N-1-(2-mercaptoethyl) adenine functionalized gold nanoparticles, Sensors Actuators B: Chem. 197 (2014) 172–176.
13. R. Shaikh, N. Memon, A.R. Solangi, H.I. Shaikh, M.H. Agheem, S.A. Ali, M.R. Shah, A. Kandhro, 2, 3-Pyridine dicarboxylic acid functionalized gold nanoparticles: insight into experimental conditions for Cr3+ sensing, Spectrochim. Acta Part A: Mol. Biomolecular Spectros. 173 (2017) 241–250.
14. Y.-.J. Lai, W.-.L. Tseng, Role of 5-thio-(2-nitrobenzoic acid)-capped gold nanoparticles in the sensing of chromium (VI): remover and sensor, Analyst 136 (13) (2011) 2712–2717.
15. S. Shahrivari, F. Faridbod, M.R. Ganjali, Highly selective and sensitive colorimetric determination of Cr3+ ion by 4-amino-5-methyl-4H-1, 2, 4-triazole-3-thiol functionalized Au nanoparticles, Spectrochim. Acta Part A: Molecular Biomol. Spectros. 191 (2018) 189–194.
16. S. Bothra, J.N. Solanki, S.K. Sahoo, Functionalized silver nanoparticles as a chemosensor for pH, Hg2+ and Fe3+ in an aqueous medium, Sensors Actuators B: Chem. 188 (2013) 937–943.
17. P.S. Mdluli, N.M. Sosibo, P.N. Mashazi, T. Nyokong, R.T. Tshikhudo, A. Skepu, E. van der Lingen, Selective adsorption of PVP on the surface of silver nanoparticles: a molecular dynamics study, 1004(1–3) (2011) 131–137.
18. N.M. Sosibo, P.S. Mdluli, P.N. Mashazi, B. Dyan, N. Revaprasadu, T. Nyokong, R.T. Tshikhudo, A. Skepu, E. Van der Lingen, Synthesis, density functional theory, molecular dynamics and electrochemical studies of 3-thiophene acetic acid-capped gold nanoparticles, 1006(1–3) (2011) 494–501.
19. M. Mlambo, R.A. Harris, P. Mashazi, M. Sabela, S. Kanchi, L.M. Madikizela, P.N. Shumbula, N. Moloto, T.T. Hlatshwayo, P.S. Mdluli, Computational and experimental evaluation of selective substitution of thiolated coumarin derivatives on gold nanoparticles: Surface enhancing Raman scattering and electrochemical studies, 396 (2017) 695–704.
20. R. Harris, M. Mlambo, P.S. Mdluli, Qualitative analysis of some alkanethiols on Au nanoparticles during SERS, 6(15) (2016) 12131–12142.

21. P.S. Mdluli, N.M. Sosibo, N. Revaprasadu, P. Karamanis, J. Leszczynski, Surface-enhanced Raman spectroscopy (SERS) and density functional theory (DFT) study for understanding the regioselective adsorption of pyrrolidinone on the surface of silver and gold colloids, 935(1–3) (2009) 32–38.
22. Y. Upadhyay, T. Anand, L.T. Babu, P. Paira, A. Kumar Sk, R. Kumar, S.K. Sahoo, Combined use of spectrophotometer and smartphone for the optical detection of Fe3+ using a vitamin B6 cofactor conjugated pyrene derivative and its application in live cells imaging, J. Photochem. Photobiol. A: Chem. 361 (2018) 34–40.
23. Y. Upadhyay, S. Bothra, R. Kumar, S.K. Sahoo, Smartphone-assisted colorimetric detection of Cr3+ using vitamin B6 cofactor functionalized gold nanoparticles and its applications in real sample analyses, ChemistrySelect 3 (24) (2018) 6892–6896.
24. S. Li, Q. Zhang, Y. Lu, D. Zhang, J. Liu, L. Zhu, C. Li, L. Hu, J. Li, Q. Liu, Gold nanoparticles on graphene oxide substrate as sensitive nanoprobes for rapid L–Cysteine detection through smartphone-based multimode analysis, Chemistry-Select 3 (35) (2018) 10 0 02–10 0 09.
25. A. Kumar, A. Bera, S. Kumar, A smartphone-assisted sensitive, selective and reversible recognition of copper ions in an aqueous medium, ChemistrySelect 5 (3) (2020) 1020–1028.
26. N. Metropolis, A.W. Rosenbluth, M.N. Rosenbluth, A.H. Teller, E. Teller, Equation of state calculations by fast computing machines, J. Chem. Phys. 21 (6) (1953) 1087–1092.
27. L. Liu, Y. Leng, H. Lin, Photometric and visual detection of Cr(VI) using gold nanoparticles modified with 1,5-diphenylcarbazide, Microchimica Acta 183 (4) (2016) 1367–1373.
28. X. Liu, J.J. Xiang, Y. Tang, X.L. Zhang, Q.Q. Fu, J.H. Zou, Y. Lin, Colloidal gold nanoparticle probe-based immunochromatographic assay for the rapid detection of chromium ions in water and serum samples, Anal Chim Acta 745 (2012) 99–105.
29. S. Li, T. Wei, G. Ren, F. Chai, H. Wu, F. Qu, Gold nanoparticles based colorimetric probe for Cr (III) and Cr (VI) detection, Colloids Surfaces A: Physicochem. Eng. Asp. 535 (2017) 215–224.
30. L. Zhao, Y. Jin, Z. Yan, Y. Liu, H. Zhu, Novel, highly selective detection of Cr (III) in aqueous solution based on a gold nanoparticles colorimetric assay and its application for determining Cr (VI), Anal. Chim. Acta 731 (2012) 75–81.
31. S.E. Magubane, M. Mlambo, M.H. Mabaso, S.F. Muthwa, H.G. Kruger, P.S. Mdluli, Optimization of CIEL∗ a∗ b∗ /Yxy colour system for colorimetric devices fabricated with gold nanoparticles, 1191 (2019) 271–277